Available online at www.sciencedirect.com
SCIENCE DIRECT®
Journal of Power Sources 130 (2004) 111–118
JOURNAL OF POWER SOURCES
www.elsevier.com/locate/jpowsour

Power generation using a mesoscale fuel cell integrated with a microscale fuel processor

J.D. Holladay [a,*], J.S. Wainright [b], E.O. Jones [a], S.R. Gano [a]

[a] *Battelle, Pacific Northwest Division, Richland, WA, USA*
[b] *Department of Chemical Engineering, Case Western Reserve University, Cleveland, OH, USA*

Received 29 October 2003; accepted 25 November 2003

Abstract

An integrated fuel reformer and fuel cell system for microscale (10–500 mW) power generation is being developed and demonstrated as an alternative to conventional batteries. In this system, thermal energy is transformed to electricity by stripping the hydrogen from the hydrocarbon fuel (reforming) and converting the hydrogen to electricity in a proton exchange membrane (PEM) fuel cell. The fabrication and operation of a mesoscale fuel cell based on phosphoric acid doped polybenzimidazole (PBI) technology is discussed, along with tests integrating the methanol processor with the fuel cell. The PBI membrane had high ionic conductivity at high temperatures (>150 °C), and sustained the high conductivity at low relative humidity at these temperatures. This high-temperature stability and high ionic conductivity enabled the membrane to tolerate extremely high levels of carbon monoxide up to 10% without significant degradation in performance. The combined fuel cell/reformer system was successfully operated to enable the production of 23 mW of electrical power.

Keywords: Proton exchange membrane fuel cells; Polybenzimidazole; Microtechnology; Fuel processing

1. Introduction

The potential for creating new, miniature, power supplies that operate with higher energy densities than batteries has prompted a range of research into alternative power sources [1–9]. One technique under investigation involves converting the high thermal energy contained in hydrocarbons (5.6 kWh/kg for methanol and 12.6 kWh/kg for diesel) into electrical energy through direct methanol fuel cells or through proton exchange membrane (PEM) fuel cells operating on pure hydrogen or on reformed hydrocarbons. With this approach, only about 4% efficiency is required to develop devices with energy densities equivalent to current Li-ion batteries; higher efficiencies would result in still greater energy densities. The technology discussed here comprises a mesoscale PEM fuel cell that works in conjunction with a microscale fuel processor (reformer). In this system, the fuel processor generates a hydrogen-rich product stream that is fed to the fuel cell—all within an anticipated 10–20 cm^3 package. A miniature methanol fuel processor has been discussed in depth previously [9]. This paper focuses primarily on the mesoscale fuel cell.

One of the major challenges to PEM fuel cell/fuel processor systems has been the low tolerance to carbon monoxide on the fuel cell anode. For conventional fuel cells, the carbon monoxide levels need to be below 10 ppm [10], which in turn requires the use of additional reactors, such as water–gas shift (WGS) and preferential oxidation (PrO_x), or membrane purifier. Compared to processors using higher hydrocarbon fuels, methanol processors have an advantage: their product stream often contains 1% or less CO on a dry gas basis. In that case, the WGS reactors can be eliminated. However, further clean-up using either a membrane or PrO_x reactor is still required. These additional reactors increase the size and complexity of the reformer system while often lowering the efficiency.

The PEM fuel cell CO tolerance has been improved to 100 ppm by raising the fuel cell temperature to 70–80 °C and by adding ruthenium to the anode [10]. It has been shown that raising the operating temperatures to >100 °C would improve the CO tolerance even further; however, at the higher temperatures the ionic conductivity of the membrane is significantly lowered due to water loss. Wainright et al. [11] have proposed the use of phosphoric acid doped polybenzimidazole (PBI) as a way to allow the fuel cell

* Corresponding author. Present address: P.O. Box 999, MS K8-93, Richland, WA 99352, USA. Fax: +1-509-376-5106.
E-mail address: jamelyn.holladay@pnl.gov (J.D. Holladay).

0378-7753/$ – see front matter © 2004 Elsevier B.V. All rights reserved.
doi:10.1016/j.jpowsour.2003.11.055

to operate at higher temperatures, thus increasing the CO tolerance of the fuel cell.

This paper discusses a mesoscale fuel cell (1–2 cm^2) developed for use in micropower generation. Experiments to determine the ionic conductivity of PBI membranes and the associated increase in CO tolerance are described, as well as fuel cell fabrication and performance. Results of tests integrating the fuel cell with a microscale fuel processor are also summarized.

2. Experimental

2.1. High-temperature membrane conductivity

The ionic conductivities of many PEM fuel cells are strongly dependent on the level of hydration [12]. Therefore, in many fuel cell systems the reactants need to be humidified in order to prevent excessive water evaporation. However, it is believed phosphoric acid will aid in the ionic conductivity and that its hydrophilic character will decrease water evaporation rates and thus the need for or degree of reactant humidification. To gain a greater understanding of the mechanism of ionic conductivity in the phosphoric acid doped PBI electrolyte, this study considered the following variables: temperature (50–200 °C), relative humidity (5–30%RH) and doping level (3–6.3 H_3PO_4 molecules per polymer repeat unit). All of the membrane electrolyte samples were cast in the doped form from trifluoroacetic acid solution using a gardner knife. The conductivity results were obtained using an in-house fabricated four-probe apparatus. This apparatus is limited to maximum pressures of 133 kPa absolute; thus, the full range of humidities could not be investigated over the full range of temperatures. Details of the casting techniques and the four-probe apparatus have been described previously [13,14].

2.2. Carbon monoxide tolerance

An extended study of CO tolerance was carried out using conventional fuel cell hardware and conventionally fabricated PBI fuel cells. The membrane electrode assembly (MEA) fabrication using electrodes from E-tek Inc. has been described previously [15]. The anode loading was 0.35 mg Pt/cm^2. The charge transfer resistance for hydrogen oxidation (Rct) was determined using ac impedance spectroscopy on cells operating as hydrogen pumps, i.e. the anode oxidized hydrogen as in the fuel cell, while the cathode evolved hydrogen. For the hydrogen oxidation experiments, the reactant gas was fed into one compartment of the fuel cell, and with pure hydrogen to the other side of the cell. The measured impedance represents the combined impedance of the anode and cathode. The impedance spectrum was acquired at the open circuit potential, with an ac amplitude of 10 mV R.M.S. over a frequency range of 20,000–0.2 Hz, at five discrete frequencies per decade, equally spaced in log frequency. Under these small amplitude conditions it was assumed that the anode and cathode overpotentials were equal when both were exposed to pure hydrogen. The cathode charge transfer resistance was then taken to be 50% of the total charge resistance measured. When the anode was exposed to hydrogen/CO mixtures, the anode charge transfer resistance was calculated by subtracting the cathode charge transfer resistance from the total charge transfer resistance. Since the cathode was not directly exposed to CO, its charge transfer resistance was assumed to be constant regardless of the anode condition.

2.3. Mesoscale fuel cell fabrication and testing

For the mesoscale device, two cells in series, each cell having an area of ≈1 cm^2, were fabricated. Using two cells in series enabled higher voltages more conducive to operating microsensors and other microelectronics. A series of thick film printing steps were used to deposit current collectors, heaters, and a Pt resistance temperature detector (RTD) on alumina, as shown in Fig. 1. The heaters were necessary to allow the cells to be tested at the appropriate temperature. Eventually, with the thermal integration of the fuel cell and the fuel processor unit, the heaters can be eliminated. The

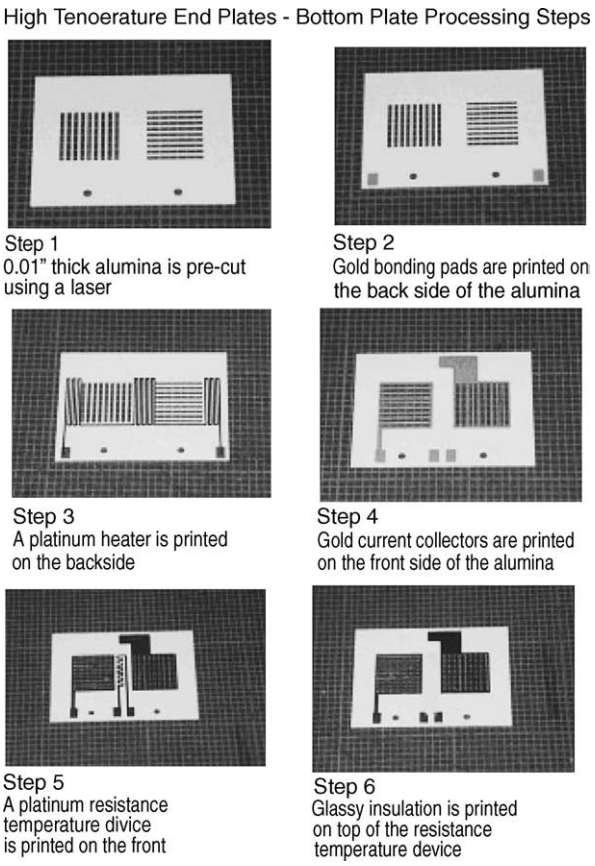

Fig. 1. Thick film processing steps for mesoscale fuel cell current collector plate.

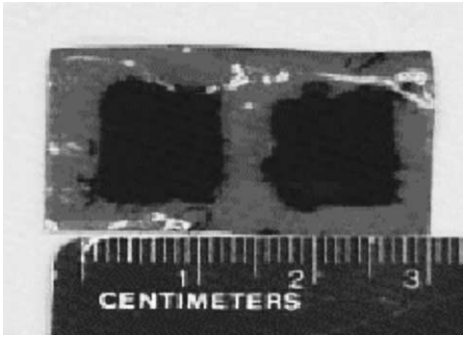

Fig. 2. Thick film printed electrodes on PBI electrolyte membrane.

RTD allows the fuel cell temperature to be monitored and the heaters controlled.

Using proprietary techniques developed at CWRU, the fuel cell electrodes (two anodes and two cathodes) were printed directly onto a PBI membrane, Fig. 2. A porous gas diffusion layer was then printed on the back of each electrode, yielding the final membrane/electrode assembly. The device was assembled by sandwiching a membrane/electrode assembly between two of the current collector plates. A high-temperature adhesive was used to hold the assembly together, and a drop of silver epoxy was used to make the series connection between the cells. The silver epoxy and the high-temperature adhesive were cured at the same time. A fuel manifold (and if desired an air manifold) constructed of alumina with 1/16 in. stainless steel tubing for the gas inlets and outlets was then bonded to the outside of the fuel cell assembly, as shown in Fig. 3. Finally, 5-mil-diameter copper wire was bonded to the contact tabs for the fuel cell leads, the heaters, and the RTD using silver epoxy. The completed fuel cell is illustrated in Fig. 4.

The fuel cell was tested at 150 °C, as measured by the RTD. Two sets of tests were completed. The first was the operation of the fuel cell with 1.2–1.7 sccm pure hydrogen. The hydrogen used was saturated with water at room temperature using a bubbler, resulting in a relative humidity of ≈1% at 150 °C. The cathode side was air breathing. The cells were operated at ambient pressure. The second test consisted of operating the fuel cell with a microscale methanol fuel processor. The fuel processor comprised a catalytic combustor, two vaporizers, a heat exchanger, and a catalytic methanol reformer, all within a volume of less than 0.25 cm^3 and a mass of less than 1 g. The volume of the reformer alone was less than 5 mm^3. A proprietary non-pyrophoric methanol reforming catalyst was used in these tests. Heat for the fuel processor was generated by the integrated catalytic combustor using methanol as the fuel. Specific details on the fuel processor fabrication, operation, and performance are described elsewhere [9]. The fuel was a 1:1 by weight mixture of methanol (Reagent Aldrich) and water that was fed to the reformer at 0.02–0.05 cm^3/h using a syringe pump. The methanol, at 0.1–0.4 cm^3/h (20 °C basis) flow, and 8–20 sccm of air were fed to the combustor.

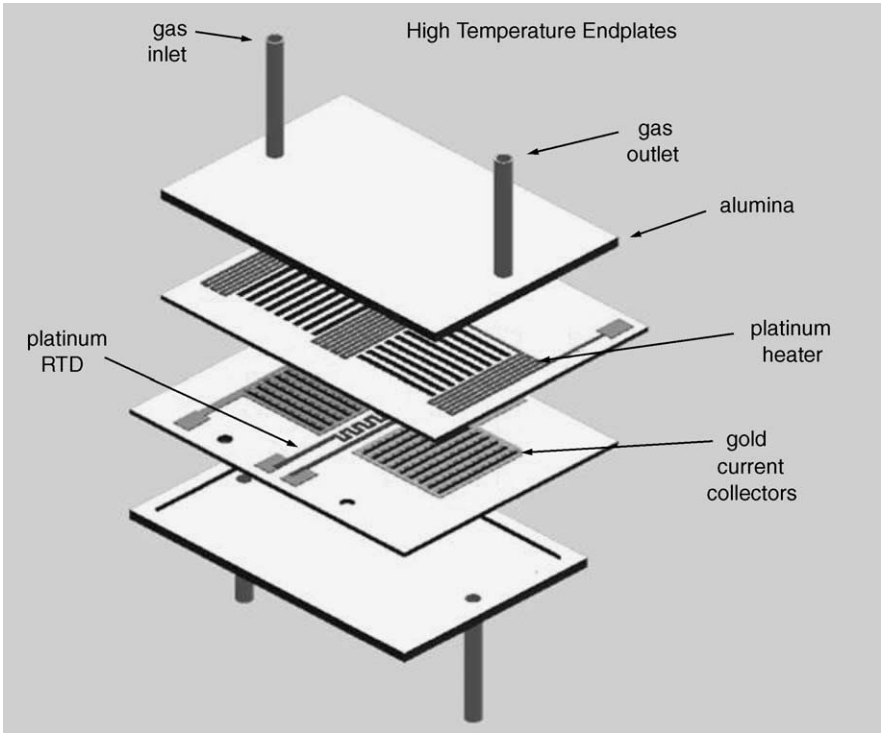

Fig. 3. Assembly of mesoscale fuel cell components. Membrane/electrode assembly (not shown) goes between the two current collector plates. Only one current collector is shown; the other cannot be seen in this view. It is located on the lower side of the first current collector plate. For air-breathing operation, only one manifold is used.

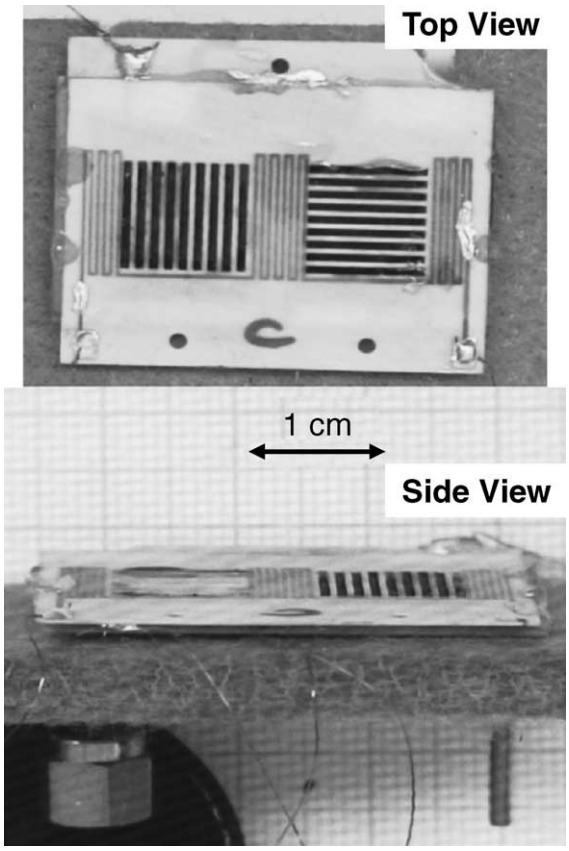

Fig. 4. Mesoscale fuel cell.

The temperature was monitored by a 0.25 mm-OD thermocouple inserted into the catalytic combustor. The temperature was maintained between 300 and 400 °C, sufficient to reform >99% of the methanol. The product gas line was manifolded to flow either to an online gas chromatograph (Agilent QuadH) for gas analysis or to the fuel cell.

3. Results and discussion

Typical results from the mesoscale fuel cell testing are discussed here, including the effect of relative humidity and doping level on membrane conductivity; PBI membrane tolerance to CO; and fabrication and tests with the fuel cell alone and integrated with a microprocessor.

3.1. Membrane conductivity

Fig. 5 illustrates the results of membrane conductivity testing, where the data have been plotted as σT versus T^{-1}. The activation energy for conduction was calculated from plots of this type. It was desired to lower the activation energy in order to increase the ionic conductivity. As evident in Table 1, the activation energy decreases with increasing doping level (molecules of H_3PO_4 per polymer repeating unit), and for the higher doping levels, decreases with increasing relative humidity. It is hypothesized that

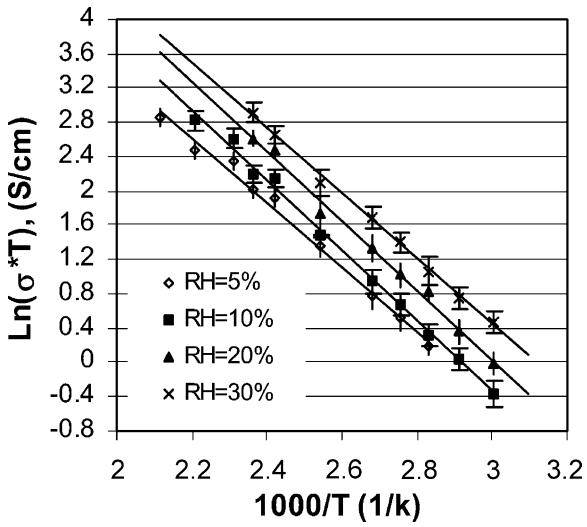

Fig. 5. Conductivity of PBI/H_3PO_4 membrane. Doping level 4.2.

higher humidity levels lower the barrier to conduction by lowering the local viscosity and by limiting the length of poly-phosphoric acid chains that arise from dehydration of H_3PO_4 [16]. Similarly, at higher doping levels, the local viscosity is lower as the local environment approaches that of the pure, liquid H_3PO_4, leading to higher conductivity.

3.2. Carbon monoxide tolerance

Fuel cells based on the PBI membrane showed very high tolerance to carbon monoxide even at extremely high concentrations of 10%, as illustrated in Fig. 6. If the typical current density for air breathing fuel cell operation is assumed to be 50 mA/cm^2 or higher, and an acceptable voltage loss due to CO is assumed to be 50 mV, then a charge transfer resistance of 1 Ω cm^2 or less is required. This condition is observed for 2% CO for temperatures above 160 °C with an anode loading of 0.35 mg Pt/cm^2. At higher CO concentrations, tolerance can be achieved by increasing the operating temperature or by increasing the Pt loading. For 10% CO, an anode Pt loading of 2 mg/cm^2 and a temperature of 185 °C is required to achieve an anode charge transfer resistance of <1 Ω cm^2.

It might be expected that increasing the humidity content in the hydrogen/CO stream would lessen the effects of CO

Table 1
Activation energy, E_a (kJ/mol) for conduction in PBI/H_3PO_4 membranes as a function of doping level (molecules of H_3PO_4 per polymer repeating unit) and relative humidity (RH)

Doping level H_3PO_4/repeat	$\sigma \times T = \sigma_0 \exp(-E_a/kT)$			
	5%RH	10%RH	20%RH	30%RH
3	32 ± 2	37 ± 3	39 ± 3	41 ± 3
4.2	31 ± 4	34 ± 4	34 ± 5	32 ± 4
5.6	30 ± 1	29 ± 1	25 ± 1	21 ± 1
6.3	28 ± 2	28 ± 2	26 ± 2	24 ± 2

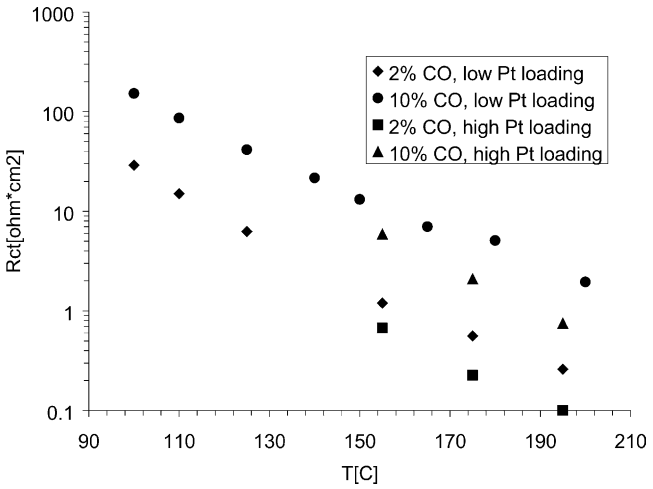

Fig. 6. Anode charge transfer resistance for PBI-based fuel cells as a function of temperature and %CO in the anode feed. Atmospheric pressure. Low platinum loading: 0.35 mg/cm^2, using 10 wt.% Pt on XC-72 catalyst. High Pt loading: 2 mg/cm^2, using 40 wt.% Pt on XC-72 catalyst.

poisoning due to (1) increased conductivity within the electrode structure leading to increased Pt utilization and/or (2) conversion of some of the CO to CO_2 via the water–gas shift reaction. To test this hypothesis, the reactant stream was saturated with water at either 25 °C or 60 °C. However, repeated experiments with these humidification conditions showed that there was not a significant effect of humidification on the hydrogen oxidation charge transfer resistance.

If the presence of CO on the catalyst surface is assumed to have no other effect than simply occupying a site that would otherwise be available for hydrogen oxidation, the CO coverage can be estimated from the variation in the charge transfer resistance. The results from the comparable analysis are shown in Fig. 7 for two different temperatures. It can be seen by comparing Fig. 7 with Fig. 6, that, although the coverage rises sharply at low CO concentrations, the electrode is considered "tolerant" to CO, even at coverages of ≈80%.

3.3. Mesoscale fuel cell testing

Three identical mesoscale fuel cells that were fabricated as described above were tested at 150 °C. The open circuit potential and current at 1 V results are summarized in Table 2.

The printed RTDs all showed linear calibration curves as expected, and the complete calibration curve can be developed from the data in Table 2. The variation in the RTD resistances in Table 1 is typical for the thick film process.

The printed heaters were expected to be 200 Ω resistances at room temperature. Most of the devices were within 5% of this value, again typical of the thick film printing process. However, in some cases, the printed heater was accidentally shorted to the anode or cathode current collector. In these cases, the heater could not be used. The shorted heaters were the result of poor mask alignment during fabrication, and have since been eliminated by re-designing the heater mask to allow for unavoidable alignment error.

For two cells in series, open circuit voltages of ≈1.8 V were expected. Two of the devices achieved this at 150 °C, while all devices measured 1.8 V or more at lower temperatures. We are continuing to investigate the cause of the drop in open circuit potential with increasing temperature (all devices showed even lower open circuit potentials at 180 °C). This phenomenon was unexpected, and may be related to the adhesives used to seal the device.

The internal resistance column reflects the sum of the resistances from the lead wires used to connect to the device, the ionic resistance of the electrolyte membrane, the electrical resistance of the current collectors and the printed

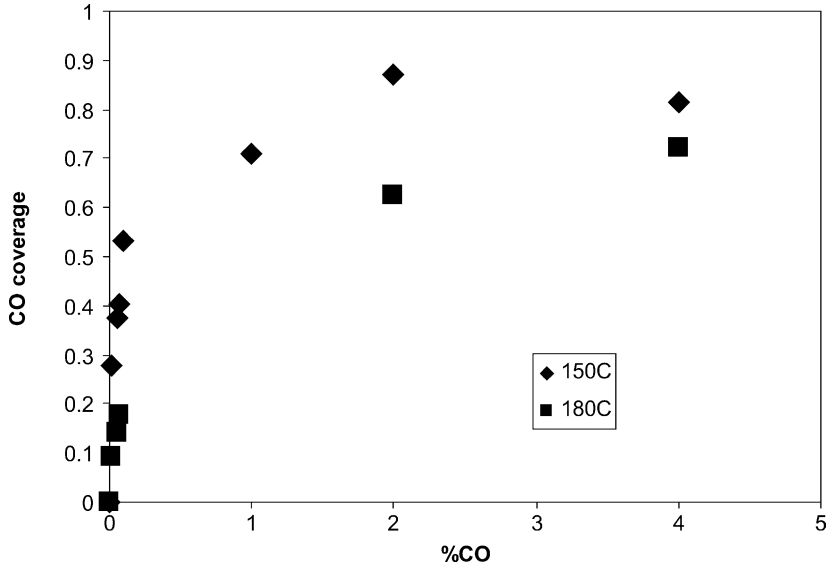

Fig. 7. Estimated CO coverage as function of CO concentration at 150 and 180 °C.

Table 2
Test results for mesoscale fuel cell devices

Device	RTD resistance at 23 °C (Ω)	RTD resistance at 150 °C (Ω)	Anode heater resistance (Ω)	Cathode heater resistance (Ω)	Open circuit voltage (V)	Internal resistance (Ω)	Current at 1 V at 150 °C (mA)
B	22.2	31.6	43.4–X	198	1.66	1.72	81
D	22.8	32.2	192	X	1.77	1.35	123
E	21.4	30.3	168	190	1.83	1.57	99

X: Heater shorted to fuel cell current collector. All fuel cell results are with ≈1.7 sccm H_2, air breathing—hot (150 °C) gases.

gas diffusion layer, and the contact resistances between the electrode assemblies and the current collectors. The membrane resistance can be estimated from separate measurements of the membrane conductivity under controlled conditions. The hydrogen gas used was saturated with water at room temperature, leading to a relative humidity of ≈1% at 150 °C. At 150 °C and 1%RH, the electrolyte conductivity is ≈0.015 S/cm, equivalent to a membrane resistance of 0.5 Ω/cell, or 1.0 Ω for the device. It should be noted that the electrical leads connected to the fuel cell were made of very fine wire to reduce thermal losses. The electrical resistance of the lead wires (roughly 15 cm of 0.127 mm diameter copper wire, two wires/device) is ≈0.3 Ω. Therefore, device D is essentially ideal; the observed internal resistance can be attributed to the known electrolyte and lead wire resistance, i.e. the contact resistances are very small. For the other devices, the contact resistances are greater, and the power output is lower.

The current output at 1 V represents the maximum electrical output, ≈100 mW, that was obtained from the mesoscale fuel cell devices using pure H_2 as the fuel. Complete polarization curves on pure H_2 are shown in Fig. 8 for the three devices listed in Table 2. The limiting currents that can be observed in Fig. 8 for devices D and E are consistent with complete utilization of the 1.7 sccm H_2 feed. The slightly lower limiting current observed for device B is thought to be the result of inaccurate control of the hydrogen flow rate by the mass flow controller used, which was rated at 1 sccm minimum controllable flow.

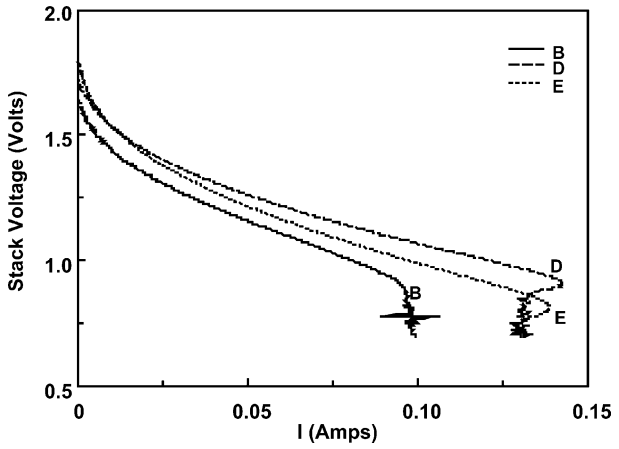

Fig. 8. Polarization curves for three different, two-cell mesofabricated devices. Temperature 150 °C. Fuel: pure H_2 at 1.7 sccm. Air breathing cathode.

In tests with the integrated fuel cell and fuel processor, the system performed according to expectations. The procedure for system start-up did not require electrical heating. Instead, hydrogen and air were fed to the combustor to initiate combustion and heat the vaporizers. Once the vaporizers were heated to approximately 80 °C, methanol for combustion was fed to the vaporizer. The hydrogen was slowly tapered off as the methanol feed was increased until only methanol and air were being fed to the combustor and the device was completely self-sustaining. The methanol/air mixture was adjusted until the steam reformer reached the desired temperatures (250–400 °C), depending on the conditions being tested. The methanol/water solution feed to the steam reformer was then initiated.

Greater than 99% methanol conversion was achieved under the operating conditions. Fig. 9 shows the conversion with temperature performance at the feed flow rate of 0.03 cm^3/h, which is representative of the other flow rates examined. Greater than 99% conversion with a feed flow of 0.05 cm^3/h was achieved at 420 °C. The typical product gas was composed of hydrogen 73–74%, carbon dioxide 23–25%, and carbon monoxide 1–2% on a dry gas basis.

A feed of 0.05 cm^3/h was supplied to the reformer to produce a hydrogen-rich gas stream with a flow of 1.1 sccm. This gas was directed to the fuel cell, which was already at ∼150 °C. A variable load was applied to the fuel cell stack, and the resulting performance is presented in Fig. 10. A maximum power output of 23 mW_e was produced. The performance was slightly lower than expected; however, it did demonstrate that a microscale power generator based on fuel processing and high-temperature fuel cells is feasible. Several factors contribute to the lower power output seen in Fig. 10 as compared to the performance shown in Fig. 8. The first is the total hydrogen supply, which was 1.7 sccm in Fig. 9, but only 0.8 sccm (73% of 1.1 sccm) for Fig. 10. As a result, the power output cannot be 100 mW as shown in Fig. 8, but at best would be ≈50 mW operating on reformate. The fuel cell performance in Fig. 8 was with neat hydrogen, whereas the fuel feed from the reformer has a significant amount of CO_2 (25%) and CO (1–2%), which would lower the performance. Assuming an anode charge transfer resistance of 1.2 Ω cm^2 (see Fig. 6, 2% CO, 15 °C, 0.35 mg Pt/cm^2), the voltage loss due to CO at the peak power point in Fig. 10 is ≈24 mV at each anode. The 25% CO_2 also has a significant influence on the performance of these devices. The printed gas diffusion layers used in the these devices are considerably less porous (30–50%

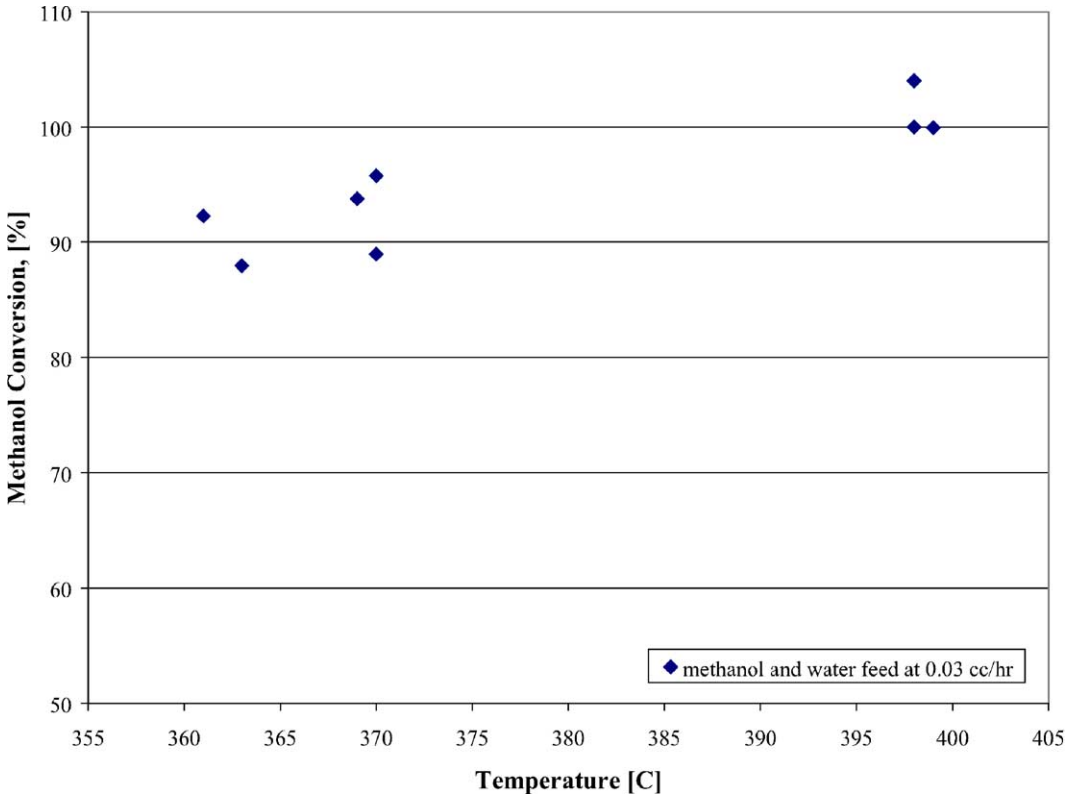

Fig. 9. Methanol conversion in the microscale fuel processor operated with a feed of 50 wt.% methanol in water.

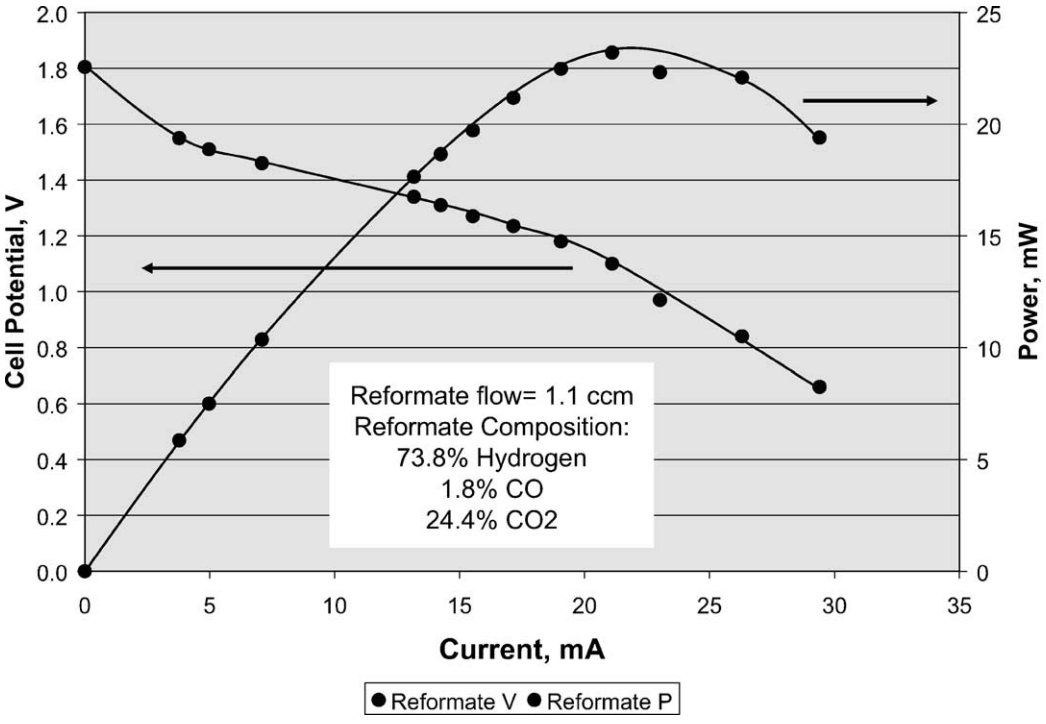

Fig. 10. Bread-boarded fuel processor and fuel cell performance.

porosity) than typical carbon cloth or carbon paper gas diffusion media (80% porosity) used for PEM fuel cells. As a result, the dilution effect of the CO_2 is magnified, lowering the power output when operating on reformate. It is believed that these effects caused the lower power.

4. Conclusions

The phosphoric acid doped PBI membrane had high ionic conductivity at high temperatures (>150 °C). The membrane was able to sustain the high conductivity at low relative humidity at these temperatures. The high-temperature stability and high ionic conductivity enabled the membrane to tolerate high levels of carbon monoxide without significant degradation in performance. A fuel cell based on this technology may be able to tolerate the product gas from a hydrocarbon reformer without significant CO clean-up. For higher hydrocarbons a WGS reactor may still be used to maximize the hydrogen production; however, the PrO_x reactors can be eliminated, simplifying the system. For methanol reformers, both the WGS and PrO_x reactors may be eliminated to further simplify the system. The flexibility of both the fuel cell technology and the reformer technology was demonstrated by the fabrication and operation of a mesoscale fuel cell based on PBI technology and a microscale methanol processor. The systems were successfully operated to enable the production of 23 mW_e of power, demonstrating that sub-watt power generation using a methanol reformer and high-temperature fuel cell system is feasible. Optimization and integration of the mesoscale fuel cell and the fuel processor should result in substantially higher efficiency and power output.

References

[1] R.F. Savinell, in: Gordon Research Conference on Electrochemistry, California, 2001.
[2] J.S. Wainright, R.F. Savinell, in: Fall International Meeting of the Electrochemical Society, Phoenix, AZ, 2000.
[3] L.M. Matta, M. Nan, S.P. Davis, D.V. McAllister, B.T. Zinn, M.G. Allen, in: American Institute of Aeronautics and Astronautics (AIAA) Paper 2001-0978, AIAA, Aerospace Sciences Meeting and Exhibition, Reno, NV, 2001.
[4] S.B. Schaevitz, A.J. Franz, K.F. Jensen, M.A. Schmidt, A, in: The 11th International Conference on Solid-State Sensors and Actuators, Munich, Germany, 2001, p. 30.
[5] K. Fu, A. Knobloch, F. Martinez, D.C. Walther, C. Fernandez-Pello, A.P. Pisano, D. Liepmann, K. Miyaska, K. Maruta, in: International Mechanical Engineering Congress and Exposition (IMECE), New York, 2001.
[6] K. Fu, A.J. Knobloch, F.C. Martinez, D.C. Walther, C. Fernandez-Pello, A.P. Pisano, D. Liepmann, in: International Mechanical Engineering Congress and Exposition (IMECE), New York, 2001.
[7] K. Maruta, K. Koichi Takeda, L. Sitzki, K. Borer, P.D. Ronney, S. Wussow, O. Deutschmann, in: Third Asia-Pacific Conference on Combustion, Seoul, South Korea, 2001.
[8] C.D. Richards, D.F. Bahr, C.-G. Xu, R.F. Richards, in: Proceedings of the IECEC 2001, 36th Intersociety Energy Conversion Engineering Conference, Savannah, GA. 2001.
[9] J.D. Holladay, E.O. Jones, M. Phelps, J. Hu, J. Power Sources 108 (2002) 21.
[10] D. Thompsett, Fuel Cell Technology Handbook, G. Hoogers (Ed.), CRC Press, New York, 2003, pp. 6–2.
[11] J.S. Wainright, J.-T. Wang, R.F. Savinell, M. Litt, J. Electrochem. Soc. 142 (1995) L121.
[12] T.A. Zawodzinski, T.E. Springer, J. Davey, R. Jestel, C. Lopez, J. Valerio, S. Gottesfeld, J. Electrochem. Soc. 140 (1993) 1981.
[13] B. Cahan, J.S. Wainright, J. Electrochem. Soc. 140 (1993) L185.
[14] M. Litt, R. Ameri, Y. Wang, R. Savinell, J. Wainright, Mater. Res. Soc. Symp. Proc. 548 (1999) 313.
[15] S.R. Samms, R.F. Savinell, J. Power Sources 112 (2002) 13.
[16] Y. Ma, J.S. Wainright, R.F. Savinell, J. Electrochem. Soc. in press.